

Fabrication of Doped Black Phosphorus Crystal by the Chemical Vapor Transport Method

Mingfu Fu, Wen Yang,* Kaixiang Du, Jiabao Li, Yong Zhang, Shukang Deng, and Peizhi Yang*

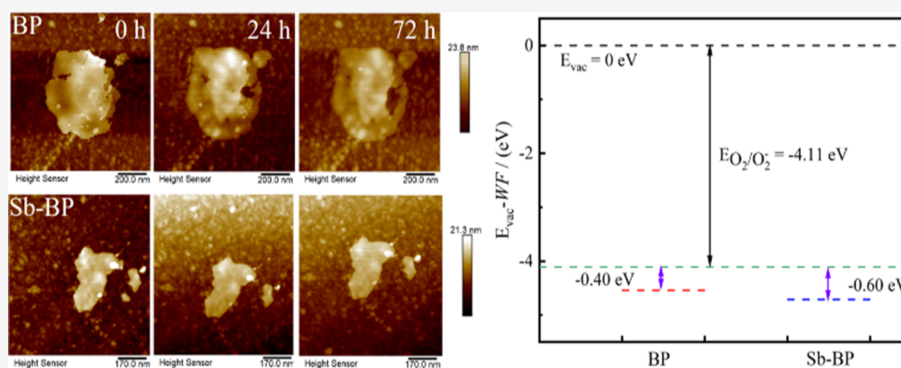
Cite This: <https://doi.org/10.1021/acs.cgd.2c00848>

Read Online

ACCESS |

Metrics & More

Article Recommendations



ABSTRACT: Black phosphorus (BP) has received growing attention due to its suitable carrier mobility and switching ratio, tunable direct band gap, and strong in-plane anisotropy. In recent years, the applied research of both bulk and few-layer BP has yielded continuous breakthroughs, while the device applications with stable performance have lagged due to their poor environmental stability. Additionally, fabricating high-quality doped BP by a desirable chemical vapor transport (CVT) method has been challenging. Herein, the CVT approach with a constant temperature was employed to fabricate Sb-doped BP (Sb-BP) and Bi-doped BP (Bi-BP) to enhance the performance of pristine BP. The characterizations, including Raman, transmission electron microscopy, atomic force microscopy, and so forth, were employed to study the phase structure and properties of the as-grown crystals. The results suggest that BP and doped BP belong to an orthorhombic structure and show good crystallinity. Distinct from pristine BP, the light absorption and electrochemical properties of orthorhombic BP were improved by doping. Furthermore, the storage time of Sb-BP exceeds 65 days, while the degradation of pristine BP occurs within 38 days in ambient condition. The degradation rate of Sb-BP was slower than that of pristine BP even in the harsh environment, which indicates that the antioxidation of Sb-BP is outstanding. Hence, doping is a viable method to modify the properties of BP. This work provides useful guidance for preparing other doped BP and BP compounds, broadening the application field of the phosphorus family.

1. INTRODUCTION

Since graphene was successfully exfoliated in 2004,¹ the research on two-dimensional materials has grown exponentially over the past decade. Graphene (GR), transition metal dichalcogenides (TMDCs), and black phosphorus (BP) as the main representatives of 2D layer materials have shown great application potential for (opto)electronic devices, energy storage, catalysis, thermoelectricity, and biological medicine, due to their excellent physical and chemical properties.² Although GR and TMDCs have achieved good applications, the intrinsic shortcomings limit their applications on certain devices.³ By contrast, BP with a suitable band gap and carrier mobility bridges the gap between GR and TMDCs, and has been identified as a promising next-generation semiconductor material. However, the large-scale application of BP has been hindered by its environmental instability. To boost the

flourishing development of BP, it is essential to develop effective strategies to mitigate the stability issue.

As we all know, doping is a common approach to modifying the band structure of materials. Despite several methods that have been employed to synthesize doped 2D materials,^{4–6} the majority of the strategies are not suitable for one-step preparation of doped BP, due to the distinction in synthesized methods for different materials. Doping BP can be achieved in several ways: the high-pressure pathway, the pulsed-plasma

Received: July 27, 2022

Revised: November 11, 2022

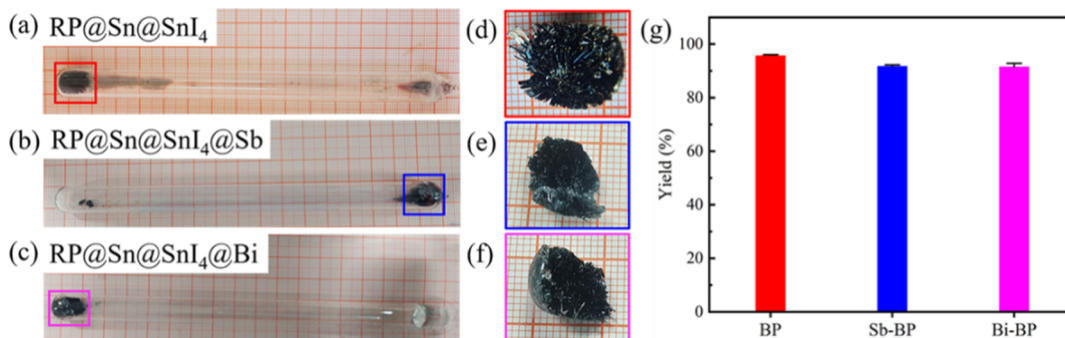


Figure 1. Bulk BP and doped BP were synthesized via the CVT method. (a) BP, (b) Sb-BP, and (c) Bi-BP, (d–f) represents corresponding cleaned products, respectively. A small grid of grid paper represents 1 mm. (g) Yield of pristine BP and doped BP.

process, electrochemical intercalation, surface charge transfer, electrostatic carrier doping, ball-milling, chemical vapor transport (CVT),^{7–9} and so forth. Among them, the CVT reaction has the advantages of low equipment requirements, simple operation, one-step synthesis, and so forth. Thus far, both heterovalent doping, such as with Se and Te, and isovalent doping, with As, Sb, and Bi, have been successfully achieved.^{9–13}

In this work, high-yield BP crystals were synthesized via the CVT method. Sb and Bi were used as dopants to generate Sb-BP and Bi-BP under the same synthesis conditions. Subsequently, a series of phase and structural characterization techniques were applied. In addition, light absorption, electrochemical properties, and antioxidation of BP and doped BP were studied. Beyond the electronic structure modification, interestingly, Sb doping has been shown to improve material stability.

2. MATERIALS AND METHODS

2.1. Materials and Reagents. Bulk red phosphorus particles (RP, 99.999%), tin particles (Sn, 99.999%), and stannic iodide powders (SnI₄, 99.998%) are used as raw materials for fabricating BP crystals. The antimony particles (Sb, 99.999%) and bismuth particles (Bi, 99.99%) are applied to yield Sb-BP and Bi-BP crystals, respectively. Among them, the Sb is bought from Shanghai Macklin Biochemical Co., Ltd other chemical reagents are bought from Shanghai Aladdin Biochemical Technology Co., Ltd. Besides the abovementioned materials, anhydrous ethanol purchased from Tianjin Zhiyuan Chemical Reagent Co., Ltd is used to clean the crystals.

2.2. Synthesis of BP and Doped BP. Bulk RP (400 mg), Sn (30 mg), SnI₄ (10 mg), Sb (10 mg), and Bi (5 mg) were used as raw materials for fabricating the crystals. The abovementioned source materials were weighed and sealed in a 12 mm diameter quartz ampoule under a vacuum. Then, the sealed ampoules were horizontally placed in a muffle furnace. Large-size orthorhombic BP and doped BP were prepared by the CVT method under a uniform temperature profile. Given the use of constant heating temperature, the reagents are not required to be placed at a specific site. These precursors were first heated to 700–750 °C for 3 h to allow the mineralizers to react completely. Subsequently, the temperature was slowly decreased to 500 °C at a rate of 0.5 °C min⁻¹ and kept at the temperature for 7 h. Finally, the heating procedure was completed, and the ampoules were cooled to room temperature naturally. The bulk BP and doped BP were obtained in the ampoules.

2.3. Material Characterization. After ultrasonic cleaning and vacuum drying, the crystal structures of the cleaned products were characterized by X-ray diffraction (XRD, Rigaku Ultimate IV) equipped with Cu K α radiation in the range of two theta from 10 to 80°. Raman measurement (Horiba LabRAM HR Evolution) with a 532 nm laser at a power of 2 mW was carried out to obtain additional information on the internal atomic vibrations, within the Raman shift

range of 10–800 cm⁻¹. Meanwhile, a slit width of 100 μ m and an integral time of 5 s were used. The purity of the crystals was analyzed by X-ray photoelectron spectroscopy (XPS, Thermo Scientific, K-Alpha+) and inductively coupled plasma optical emission spectrometry (ICP-OES, NYSE: A, Agilent 5110). The surface morphology of as-grown crystals was observed using scanning electron microscopy (SEM, Hitachi, SU8010). Microstructure and single-crystal structures were observed via high-resolution transmission electron microscopy (HRTEM, JEOL, JEM-2100) on the nanosheets dripped copper mesh. The light absorption characteristics were measured by ultraviolet–visible spectrophotometry (UV-vis, Shimadzu, UV3600). Electrochemical impedance (EIS) was measured by a multichannel electrochemical workstation (DH7006, Donghua Analytical). Mechanically exfoliated flakes exposed to 85 °C and 85% relative humidity (RH = 85%) were transferred onto the Si wafer for research of the antioxidant property by atomic force microscopy (AFM, NSK, SPA-400). The ambient stability of BP and doped BP were monitored by the metallographic microscope (Leica, DM6000M). The work functions of BP and Sb-BP were acquired by the Kelvin probe system (KP Technology) in the ambient environment.

3. RESULTS

Both bulk BP and doped BP synthesized by the CVT method are shown in Figure 1. Based on the experience of previous work, appropriate ratios of mineralizers were employed during the preparation of BP and doped BP. As shown in Figure 1a–c, the precursors' transformation is relatively complete without by-products. As can be seen from Figure 1d–f, a black metallic luster can be observed on the surface of the bulk BP, and doped BP consisted of plentiful stacked bands or sheets, which is related to the fact that BP is a layered material.¹⁴ Even though BP is doped, layered property is still apparent. In addition, the pristine BP was obtained with a size of 1.3 cm. The sizes of Sb-BP and Bi-BP were also more than 1 cm by using the same parameter. According to formulas 1 and 2, the yield of BP and doped BP reaches 96% and more than 90% (Figure 1g), respectively.

$$w_{\text{BP}} = \frac{\text{mass of BP}}{\text{mass of RP}} \times 100\% \quad (1)$$

$$w_{\text{doped BP}} = \frac{\text{mass of doped BP}}{\text{mass of RP} + \text{mass of dopant}} \times 100\% \quad (2)$$

BP has six Raman active vibration modes, but only three are allowed in the commonly adopted backscattering geometry.^{15–17} In Figure 2a, three Raman active vibration peaks located at 361.66, 439.00, and 466.72 cm⁻¹ were observed in pristine BP and doped BP, which matches with the A_g¹, B_{2g},

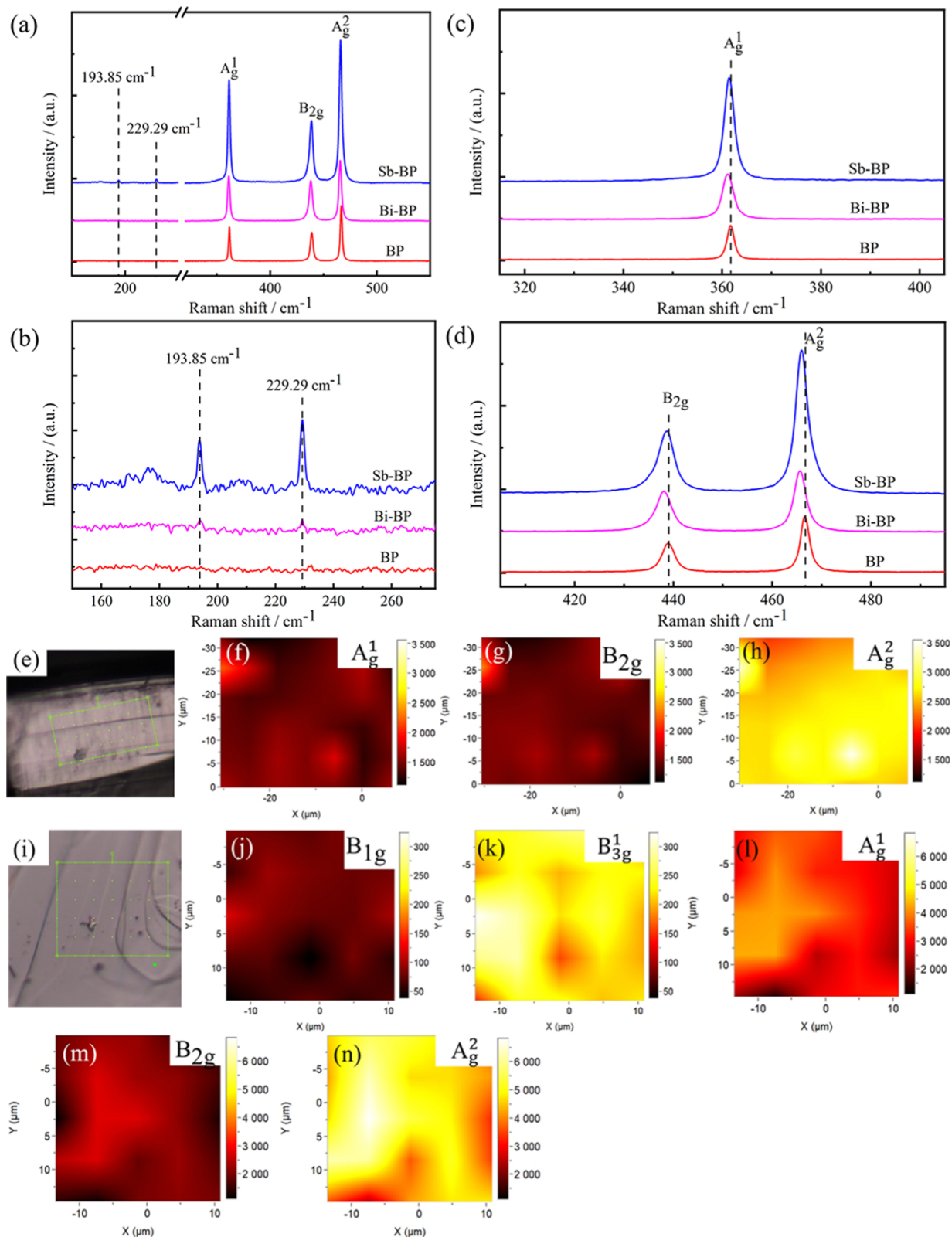


Figure 2. Raman spectra of pristine BP and doped BP. (a) Raman spectra of BP, Sb-BP, and Bi-BP. (b–d) Partial enlargement of B_{1g} , B_{3g}^1 , A_g^1 , B_{2g} , and A_g^2 , respectively. (e) Microscope image of the undoped BP and (f–h) Raman intensity mapping results for different vibration modes. (i) Microscope image of the Sb-BP and (j–n) Raman intensity mapping results for different vibration modes.

and A_g^2 vibrational modes of pristine BP, respectively. Among them, A_g^1 is primarily an out-of-plane vibration mode, B_{2g} is the vibration mode in the zigzag direction, and A_g^2 is the vibration mode in the armchair direction.^{18–20} The coexistence

of these Raman peaks is an obvious feature of orthorhombic BP,²¹ indicating that doped BP also belongs to the orthorhombic system as well as BP. The biggest difference lies in Figure 2b, two new peaks are marked as the edge

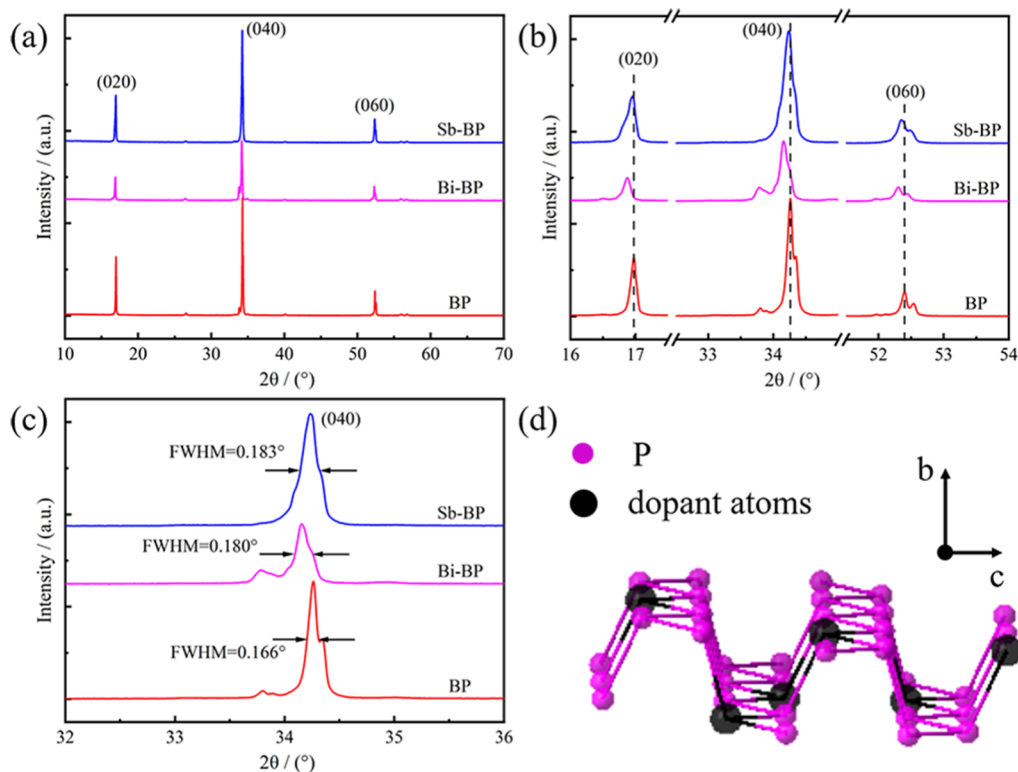


Figure 3. XRD patterns of BP and doped BP crystals. (a) XRD patterns of BP, Sb-BP, and Bi-BP. (b) Enlarged diffraction peaks of (020), (040), and (060) crystal planes. (c) Half width of the (040) diffraction peak. (d) Crystal structure of doped BP.

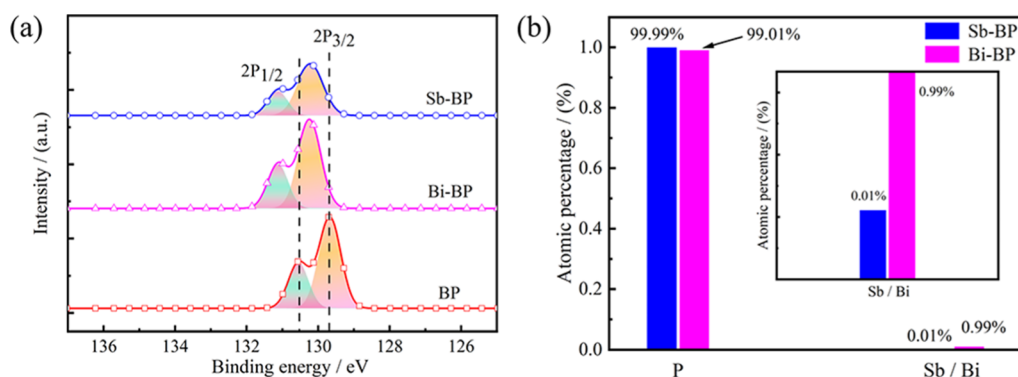


Figure 4. Phase composition analysis of BP and doped BP. (a) P 2p spectra and (b) ICP-OES measurements for BP and doped BP.

phonon vibrational modes of BP that appeared at 193.85 and 229.29 cm^{-1} after doping, which belong to B_{1g} and B_{3g}^1 forbidden in pristine BP,^{9,19} respectively. Furthermore, the three Raman peaks of A_g^1 , B_{2g} , and A_g^2 in the doped BP samples are slightly red-shifted by 0.51, 0.49, and 0.99 cm^{-1} for Sb-BP (by 0.51, 0.99, and 0.99 cm^{-1} for Bi-BP), respectively (Figure 2c,d). To visually observe the vibration intensity of each characteristic vibration peak, Raman surface scanning was carried out for the pristine BP and Sb-BP characteristic peaks. The optical microscope images of the surface-scanning region are shown in Figure 2e,i, and the surface-scanning results are shown in Figure 2f-h,j-n, respectively. It can be seen from the figures that A_g^2 has the most obvious vibration. Moreover, the B_{3g}^1 vibrates more intensely than B_{1g} , which is consistent with Figure 2b.

The crystal-structure characterizations of BP and doped BP are shown in Figure 3. The XRD pattern of as-grown materials (Figure 3a) shows that there are three diffraction peaks at

16.98, 34.27, and 52.40°, corresponding to the (020), (040), and (060) crystal planes of orthorhombic BP, respectively. The result reveals that the crystal structure of orthorhombic BP remains the same after doping Sb and Bi, with no major lattice distortion. Notably, the crystal-plane orientations of BP and doped BP are relatively consistent, mainly stacked along the *b*-axis direction, which reveals that orthorhombic BP and doped BP have the same growth characteristic with the preferred orientation of the (0*k*0) crystal plane. Besides, the crystal diffraction peaks of doped BP in Figure 3a are the same as the undoped BP, and the crystal diffraction peak of other substances do not appear, indicating that the products are doped BP rather than P-Sb alloy and P-Bi alloy. However, the diffraction peaks of doped BP are shifted toward a smaller angle than those of pristine BP in Figure 3b. Among them, for Sb-BP, the diffraction peaks of (020), (040), and (060) are slightly shifted by 0.02, 0.04, and 0.05°, respectively (by 0.10, 0.11, and 0.09° for Bi-BP), which is consistent with previous

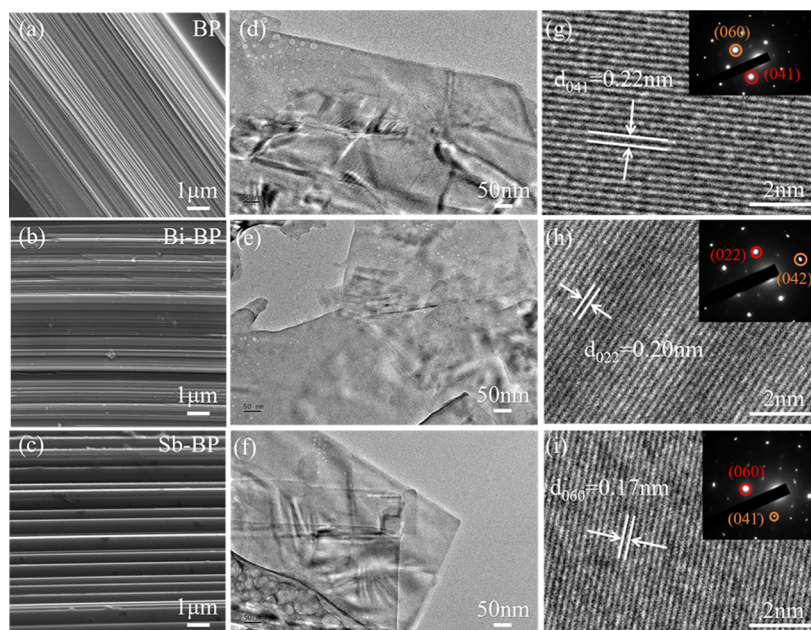


Figure 5. Surface morphology and microstructure of BP and doped BP. The SEM images of (a) BP, (b) Bi-BP, and (c) Sb-BP. The TEM images of (d) BP, (e) Bi-BP, and (f) Sb-BP. The HRTEM images and SAED patterns of (g) BP, (h) Bi-BP, and (i) Sb-BP.

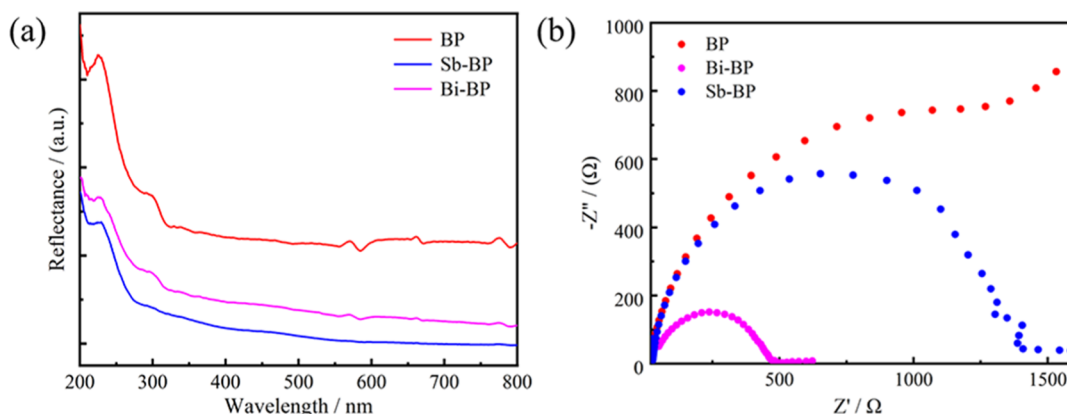


Figure 6. The properties characterization of BP and doped BP. (a) UV-vis DRS of BP, Sb-BP, and Bi-BP. (b) EIS spectrum of BP, Sb-BP, and Bi-BP.

literature reported.⁹ The result is related to the lattice expansion of BP caused by the larger atomic radius of dopant than P atomic radius.¹¹ What is more, the XRD patterns of as-grown materials exhibit sharp diffraction peaks in Figure 3a,c. The full width half maximum (FWHM) of the (040) crystal plane of the pristine BP is only 0.166° in Figure 3c. Moreover, the FWHM of doped BP was slightly larger than that of pristine BP, but the values remain relatively small, Sb-BP 0.183° and Bi-BP 0.180° , respectively. The results suggest that BP and doped BP have good crystallinity.

Figure 4 compares the XPS results of the pure BP crystals with those of doped crystals. P 2p spectrum (Figure 4a) displays the coexistence of $2p_{3/2}$ and $2p_{1/2}$ peaks at 129.67 and 130.55 eV, which is one of the characteristics of orthorhombic BP.^{21,22} This further proves the as-grown crystals have an orthorhombic structure and keep this property after doping. Moreover, there is no P-O bond near 134 eV, indicating that the as-grown samples were not significantly oxidized by H₂O and O₂.^{23–25} Compared with undoped BP, the $2p_{3/2}$ and $2p_{1/2}$ peaks of doped BP shifted by 0.56 and 0.53 eV to the higher

binding energy, respectively. The decrease in the density of the outer orbital electron cloud of P atoms in the doped BP lattice can be used to explain this phenomenon. When the density of the outer electrons decreases, the shielding effect of the outer electrons on the inner electrons will be weakened, and eventually, the binding energy of P atoms in the doped BP will increase. The ICP-OES test reveals that the atomic doping ratios of Sb and Bi are 0.01 and 0.99%, respectively (Figure 4b). All in all, doping by the constant-temperature CVT method is successful, which suggests that other BP compounds can also be synthesized via the CVT approach.

To characterize the morphology of the orthorhombic crystals, SEM and TEM were used to observe their microstructures. It can be seen from the SEM images (Figure 5a–c) that the BP and doped BP surfaces are smooth and flat with an obvious layered structure, which is consistent with the layered property of BP. In addition, the layered stack structure can be clearly seen in the low-resolution TEM images in Figure 5d–f. Clear and complete lattice fringes with defect-free lattices appear in HRTEM (Figure 5g–i) after doping,

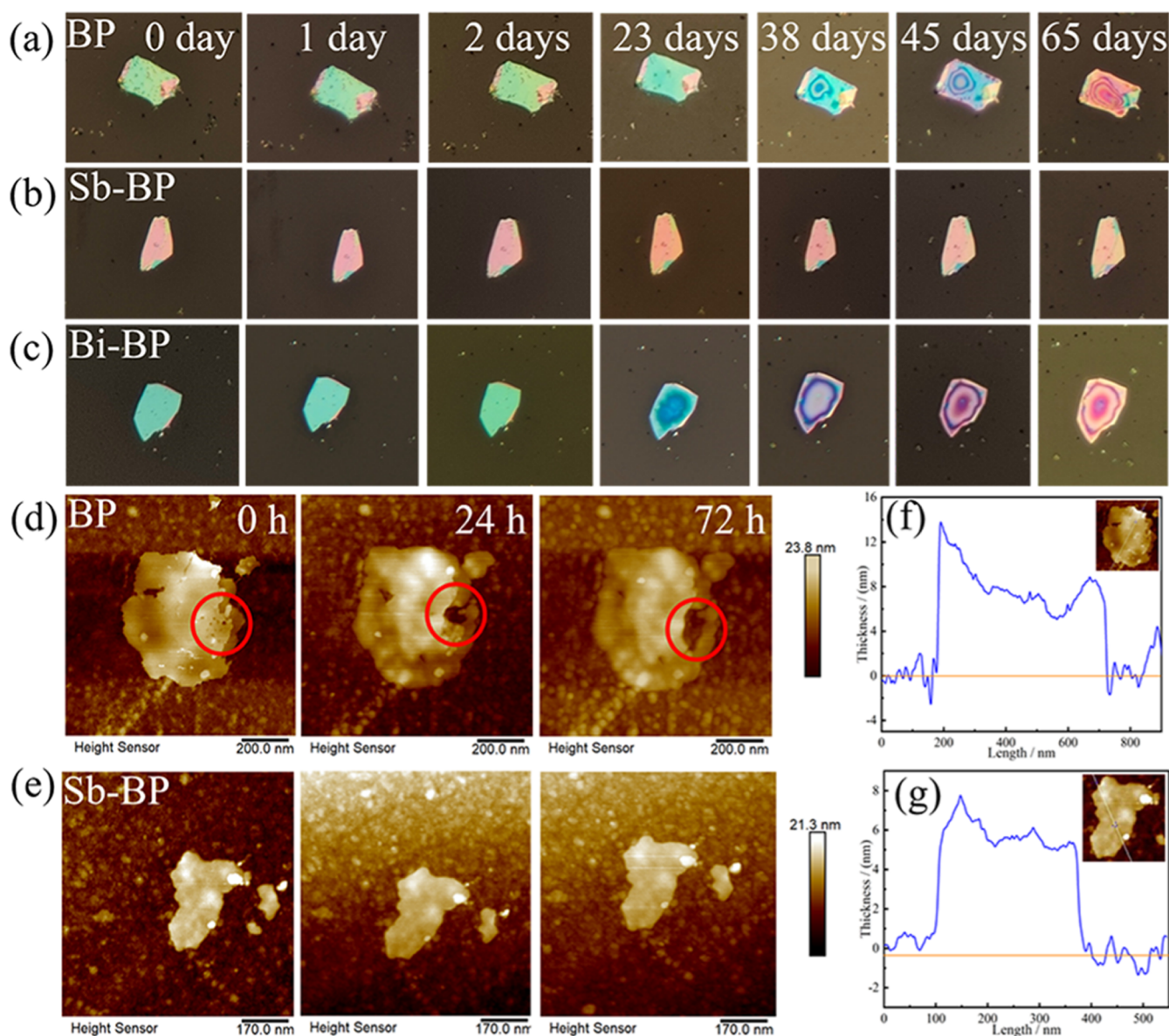


Figure 7. Environmental stability of BP and doped BP. (a–c) Surface morphology of BP and doped BP changes with time under ambient condition, (d,e) AFM photographs of BP and Sb–BP sheets exposed to 85 °C and 85% RH, and (g,h) thickness of the sheet is 8 nm in un-doped BP and 6 nm in Sb–BP.

suggesting that doping does not alter the lattice structure of BP, and the doped BP has good crystallinity. In undoped BP, the d -spacing of the lattice plane is 0.22 nm perfectly matches the (041) lattice plane, the crystal plane spacing $d_{(060)}$ is 0.17 nm in Sb–BP, and $d_{(022)}$ is 0.20 nm in Bi–BP. The corresponding selected area electron diffraction (SAED) spots are neatly arranged, clear, and bright, revealing that the as-grown crystals have the single-crystal characteristic.

Doping can effectively regulate the optical and electrochemical properties of BP. The UV–visible diffuse reflectance spectra (DRS) of the crystals are shown in Figure 6a. As can be seen from the figure, the diffuse reflection of doped BP is weaker than that of pristine BP, indicating that the doped BP has better light absorption intensity in the visible spectral range. Their EIS spectrum is recorded in Figure 6b. In Figure 6b, the impedance of pristine BP is the largest, and the transmission resistance of BP decreases after doping. Therefore, it can be seen that the electronic transmission resistance

of doped BP is small, suggesting the interfacial charge transfer efficiency of the electrodes is higher by doping, which is conducive to the expansion of BP photoelectric and catalytic applications. To sum up, the optical and electrochemical properties of BP are improved by doping.

Despite having high thermodynamic stability, thin-layer BP is known to be easily oxidized in the air.²⁴ A good match between the BP band gap and O_2/O_2^- is identified as a non-negligible factor in low ambient stability.²⁶ Previous research suggested that when the atomic doping level of Sb and Bi was 4.0%, the bottom of the conduction band of doped BP was below O_2/O_2^- redox potential, which would enhance the stability of the thin-layer BP.²⁷ However, Liu et al.⁹ reported that the ambient stability of Bi–BP was poorer than that of pristine BP. Therefore, to find out the environmental stability of the crystals, metallographic microscopy and AFM were employed to probe the morphology of the crystals in specific environment. The test results are shown in Figure 7. In Figure

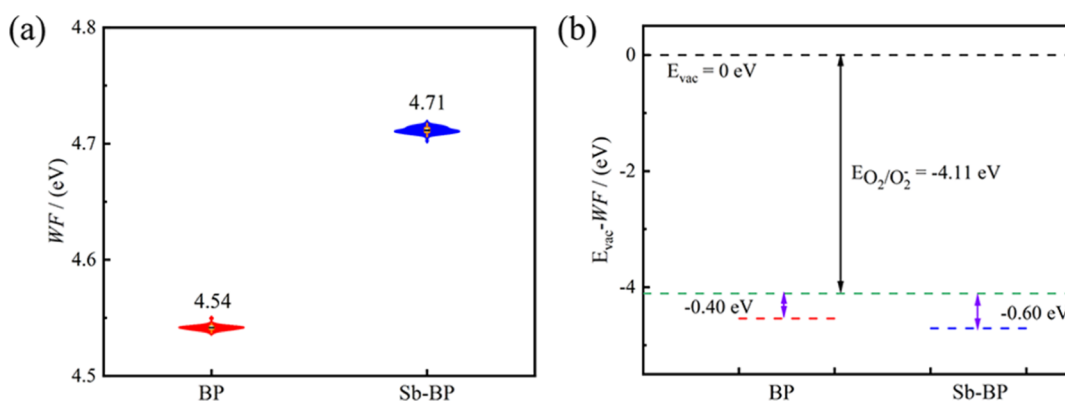


Figure 8. WF of BP and doped BP exposed to ambient condition and the relationship between E_f and E_{vac} . (a) WF of BP and Sb-BP and (b) relationship between E_f and E_{vac} of BP and Sb-BP.

7a–c, the surface color of Sb-BP sheets remains nearly unchanged after storage under ambient condition for 65 days. Unfortunately, the surface color of Bi-BP sheets changed significantly within 23 days, which is an obvious sign of degradation of the sheets. In contrast, the surface color of BP sheets exhibited little degradation after 23 days. Therefore, the Sb-BP has higher ambient stability than BP and Bi-BP. To further confirm the high stability of Sb-BP, the AFM photographs of BP and Sb-BP in a harsh environment ($T = 85\text{ }^\circ\text{C}$ and $\text{RH} = 85\%$) are shown in Figure 7d,e. The surface of freshly peeled BP and Sb-BP flakes is smooth (Figure 7d,e). After 24 h, the surface of pristine BP became rough and formed holes due to corrosion by H_2O and O_2 . With the prolonging of exposure time in a harsh environment, the surface of BP becomes rougher, and the size of the hole increases significantly, as shown in Figure 7d, which is an obvious sign of degradation. In contrast, the shape of Sb-BP flakes did not change significantly during 72 h (Figure 7e). The results are verified with Figure 7a,b, which again demonstrates that Sb-BP has higher stability, which is consistent with previous literature reports.⁹ Hence, doping with appropriate elements can not only regulate the performance of pristine BP but also improve its environmental stability.

$$\text{WF} = E_{vac} - E_f \quad (3)$$

The work function (WF) of a semiconductor, as a physical quantity, can reflect its electronic transmission capacity. The WF of BP and Sb-BP was measured by the Kelvin probe system of KP Technology at ambient condition. It can be seen from Figure 8a that the WF of BP is 4.54 eV, which is close to the value previously reported in the literature.²⁸ Also, the WF of Sb-BP is 4.71 eV. According to formula 3, the WF is the difference between the vacuum level (E_{vac}) and Fermi level (E_f), where $E_{vac} = 0\text{ eV}$, so WF can indirectly reflect the relationship between E_f and E_{vac} of the material. The relationship between E_f and E_{vac} is shown in Figure 8b, where the E_f of BP is the closest to the redox potential of O_2/O_2^- (-4.11 eV), indicating the electrons in the BP conduction band are easily transferred to O_2 to form O_2^- ; hence, the environmental stability of the pristine BP is poorer and easy to be corroded by H_2O and O_2 . However, the E_f of Sb-BP is far from the O_2/O_2^- redox potential, indicating that the stability of BP can be improved by doping. Among this, doping can adjust the energy level matching relationship between BP and O_2/O_2^- redox potential, thus improving the antioxidant of BP. On the other hand, the E_f of the semiconductor material can be seen as

the filling level of electrons. The E_f of BP decreases after doping, indicating that the BP's surface electron density declines, which is consistent with XPS results. Moreover, the Sb-BP has a lower affinity for O_2 and H_2O due to the reduction of lone pair electrons on its surface. Therefore, Sb-BP has superior ambient stability.

4. CONCLUSIONS

In conclusion, we have successfully synthesized high-yield BP, Sb-BP, and Bi-BP by the CVT method with a uniform temperature profile. A series of structural measurements show that both BP and doped BP have good crystallinity and an orthorhombic structure. Moreover, the light absorption and electrochemical properties of BP can be regulated by doping. Attractively, the crystal structure of Sb-BP is minimally degraded after storage under ambient condition for 65 days, owing to the doping. The phenomenon is similar even in harsh environment. Based on the results, doping by the CVT method is considered a viable strategy to modulate the electronic properties of BP, certainly broadening the applications of BP and its composites.

AUTHOR INFORMATION

Corresponding Authors

Wen Yang – Key Laboratory of Advanced Technique & Preparation for Renewable Energy Materials, Ministry of Education, Yunnan Normal University, Kunming 650500, P. R. China; Email: wenyang1972@hotmail.com

Peizhi Yang – Key Laboratory of Advanced Technique & Preparation for Renewable Energy Materials, Ministry of Education, Yunnan Normal University, Kunming 650500, P. R. China; Email: pzyang@hotmail.com

Authors

Mingfu Fu – Key Laboratory of Advanced Technique & Preparation for Renewable Energy Materials, Ministry of Education, Yunnan Normal University, Kunming 650500, P. R. China; orcid.org/0000-0002-8177-8492

Kaixiang Du – School of Materials Science and Engineering, Jiangsu University, Zhenjiang 212013, P. R. China

Jiabao Li – Key Laboratory of Advanced Technique & Preparation for Renewable Energy Materials, Ministry of Education, Yunnan Normal University, Kunming 650500, P. R. China

Yong Zhang – Department of Electrical and Computer Engineering and Center for Optoelectronics, University of

North Carolina at Charlotte, Charlotte, North Carolina 28223, United States; orcid.org/0000-0003-4781-1583
Shukang Deng – Key Laboratory of Advanced Technique & Preparation for Renewable Energy Materials, Ministry of Education, Yunnan Normal University, Kunming 650500, P. R. China

Complete contact information is available at:
<https://pubs.acs.org/10.1021/acs.cgd.2c00848>

Author Contributions

W.Y. and P.Y. designed and directed the study. M.F. performed the preparation of BP and doped BP crystals with the help of K.D. M.F. and J.L. wrote the manuscript. S.D. provided help with the growth of single crystals. Y.Z. assisted with test characterizations and article revisions. P.Y. provided financial support for the experimental work. All authors have approved the final version of the manuscript. These authors contributed equally.

Notes

The authors declare no competing financial interest.

ACKNOWLEDGMENTS

This work was supported by the National Natural Science Foundation of China (U1802257), the Key Applied Basic Research Program of Yunnan Province (202201AS070023), the Spring City Plan: the High-level Talent Promotion and Training Project of Kunming (2022SCP005), and the Scientific Research Fund of the Yunnan Provincial Department of Education (2022Y188).

REFERENCES

- (1) Novoselov, K. S.; Geim, A. K.; Morozov, S. V.; Jiang, D.; Zhang, Y.; Dubonos, S. V.; Grigorieva, I. V.; Firsov, A. A. Electric Field Effect in Atomically Thin Carbon Films. *Science* **2004**, *306*, 666–669.
- (2) Chang, C.; Chen, W.; Chen, Y.; Chen, Y.; Ding, F.; Fan, C.; Hagaman, D. Recent Progress on Two-Dimensional Materials. *Acta Phys.-Chim. Sin.* **2021**, *37*, 2108017.
- (3) Azadmanjiri, J.; Srivastava, V. K.; Kumar, P.; Sofer, Z.; Min, J.; Gong, J. Graphene-Supported 2D Transition Metal Dichalcogenide Van Der Waals Heterostructures. *Appl. Mater. Today* **2020**, *19*, 100600.
- (4) Mateti, S.; Glushenkov, A. M.; Li, L. H.; Ma, Q.; Zhi, C.; Chen, Y. In Situ Doping and Synthesis of Two-Dimensional Nanomaterials Using Mechano-Chemistry. *Nanoscale Horiz.* **2019**, *4*, 642–646.
- (5) Fan, S.; Tang, X.; Zhang, D.; Hu, X.; Liu, J.; Yang, L.; Su, J. Ambipolar and n/p-Type Conduction Enhancement of Two-Dimensional Materials by Surface Charge Transfer Doping. *Nanoscale* **2019**, *11*, 15359–15366.
- (6) Yoo, H.; Heo, K.; Ansari, M. H. R.; Cho, S. Recent Advances in Electrical Doping of 2D Semiconductor Materials: Methods, Analyses, and Applications. *Nanomaterials* **2021**, *11*, 832.
- (7) Yang, B.; Wan, B.; Zhou, Q.; Wang, Y.; Hu, W.; Lv, W.; Chen, Q.; Zeng, Z.; Wen, F.; Xiang, J.; Yuan, S.; Wang, J.; Zhang, B.; Wang, W.; Zhang, J.; Xu, B.; Zhao, Z.; Tian, Y.; Liu, Z. Te-Doped Black Phosphorus Field-Effect Transistors. *Adv. Mater.* **2016**, *28*, 9408–9415.
- (8) Hu, H.; Shi, Z.; Khan, K.; Cao, R.; Liang, W.; Tareen, A. K.; Zhang, Y.; Huang, W.; Guo, Z.; Luo, X.; Zhang, H. Recent Advances in Doping Engineering of Black Phosphorus. *J. Mater. Chem. A* **2020**, *8*, 5421–5441.
- (9) Liu, M.; Feng, S.; Hou, Y.; Zhao, S.; Tang, L.; Liu, J.; Wang, F.; Liu, B. High Yield Growth and Doping of Black Phosphorus with Tunable Electronic Properties. *Mater. Today* **2020**, *36*, 91–101.
- (10) Xu, Y.; Yuan, J.; Fei, L.; Wang, X.; Bao, Q.; Wang, Y.; Zhang, K.; Zhang, Y. Selenium-Doped Black Phosphorus for High-Responsivity 2D Photodetectors. *Small* **2016**, *12*, 5000–5007.
- (11) Zhang, Z.; Khurram, M.; Sun, Z.; Yan, Q. Uniform Tellurium Doping in Black Phosphorus Single Crystals by Chemical Vapor Transport. *Inorg. Chem.* **2018**, *57*, 4098–4103.
- (12) Viti, L.; Politano, A.; Zhang, K.; Vitiello, M. S. Thermoelectric Terahertz Photodetectors Based on Selenium-Doped Black Phosphorus Flakes. *Nanoscale* **2019**, *11*, 1995–2002.
- (13) Wang, J.; Zhu, J.; zhi, T.; Yang, G.; Xue, J.; Liu, B.; Chen, D.; Zhang, R.; Zheng, Y. High-Performance Sub-10 nm Monolayer Black Arsenic Phosphorus Tunneling Transistors. *Appl. Surf. Sci.* **2022**, *576*, 151705.
- (14) Yu, Q.; Guo, K.; Dai, Y.; Deng, H.; Wang, T.; Wu, H.; Xu, Y.; Shi, X.; Wu, J.; Zhang, K.; Zhou, P. Black Phosphorus for Near-Infrared Ultrafast Lasers in the Spatial/Temporal Domain. *J. Phys.: Condens. Matter* **2021**, *33*, 503001.
- (15) Sugai, S.; Ueda, T.; Murase, K. Pressure Dependence of the Lattice Vibration in the Orthorhombic and Rhombohedral Structures of Black Phosphorus. *J. Phys. Soc. Jpn.* **1981**, *50*, 3356–3361.
- (16) Ribeiro, H. B.; Villegas, C. E. P.; Bahamon, D. A.; Muraca, D.; Castro Neto, A. H.; de Souza, E. A. T.; Rocha, A. R.; Pimenta, M. A.; de Matos, C. J. S. Edge Phonons in Black Phosphorus. *Nat. Commun.* **2016**, *7*, 12191.
- (17) Mao, N.; Zhang, S.; Wu, J.; Zhang, J.; Tong, L. Lattice Vibration and Raman Scattering in Anisotropic Black Phosphorus Crystals. *Small Methods* **2018**, *2*, 1700409.
- (18) Yu, Y.; Xing, B.; Wang, D.; Guan, L.; Niu, X.; Yao, J.; Yan, X.; Zhang, S.; Liu, Y.; Wu, X.; Sha, J.; Wang, Y. Improvement in the Quality of Black Phosphorus by Selecting a Mineralizer. *Nanoscale* **2019**, *11*, 20081–20089.
- (19) Fei, R.; Yang, L. Lattice Vibrational Modes and Raman Scattering Spectra of Strained Phosphorene. *Appl. Phys. Lett.* **2014**, *105*, 199–202.
- (20) Zhang, Z.; Xin, X.; Yan, Q.; Li, Q.; Yang, Y.; Ren, T.-L. Two-Step Heating Synthesis of Sub-3 Millimeter-Sized Orthorhombic Black Phosphorus Single Crystal by Chemical Vapor Transport Reaction Method. *Sci. China Mater.* **2016**, *59*, 122–134.
- (21) Chen, Z.; Zhu, Y.; Lei, J.; Liu, W.; Xu, Y.; Feng, P. A Stage-by-Stage Phase-Induction and Nucleation of Black Phosphorus from Red Phosphorus under Low-Pressure Mineralization. *CrystEngComm* **2017**, *19*, 7207–7212.
- (22) Kang, J.; Wood, J. D.; Wells, S. A.; Lee, J.-H.; Liu, X.; Chen, K.-S.; Hersam, M. C. Solvent Exfoliation of Electronic-Grade, Two-Dimensional Black Phosphorus. *ACS Nano* **2015**, *9*, 3596–3604.
- (23) Wu, Z.; Lyu, Y.; Zhang, Y.; Ding, R.; Zheng, B.; Yang, Z.; Lau, S. P.; Chen, X. H.; Hao, J. Large-Scale Growth of Few-Layer Two-Dimensional Black Phosphorus. *Nat. Mater.* **2021**, *20*, 1203–1209.
- (24) Zhao, L.; Chao, X.; Xu, N.; Ling, G.; Zhang, P. Strategies and Applications for Improving the Stability of Black Phosphorus in Physical Environment. *Adv. Eng. Mater.* **2021**, *23*, 2100450.
- (25) Druenen, M. Degradation of Black Phosphorus and Strategies to Enhance Its Ambient Lifetime. *Adv. Mater. Interfaces* **2020**, *7*, 2001102.
- (26) Qionghua, Z.; Qian, C.; Yilong, T.; Jinlan, W. Light-Induced Ambient Degradation of Few-Layer Black Phosphorus: Mechanism and Protection. *Angew. Chem., Int. Ed.* **2016**, *55*, 11437–11441.
- (27) Lei, S.; Sun, X.; Shen, H. The Effect of Adatom Concentration on the Oxidation Reaction of Phosphorene. *Mater. Res. Express* **2018**, *6*, 025905.
- (28) Liao, W.; Wang, L.; Chen, L.; Wei, W.; Zeng, Z.; Feng, X.; Huang, L.; Tan, W. C.; Huang, X.; Ang, K. W.; Zhu, C. Efficient and Reliable Surface Charge Transfer Doping of Black Phosphorus via Atomic Layer Deposited MgO toward High Performance Complementary Circuits. *Nanoscale* **2018**, *10*, 17007–17014.